X-rays from the Sun and the Stars

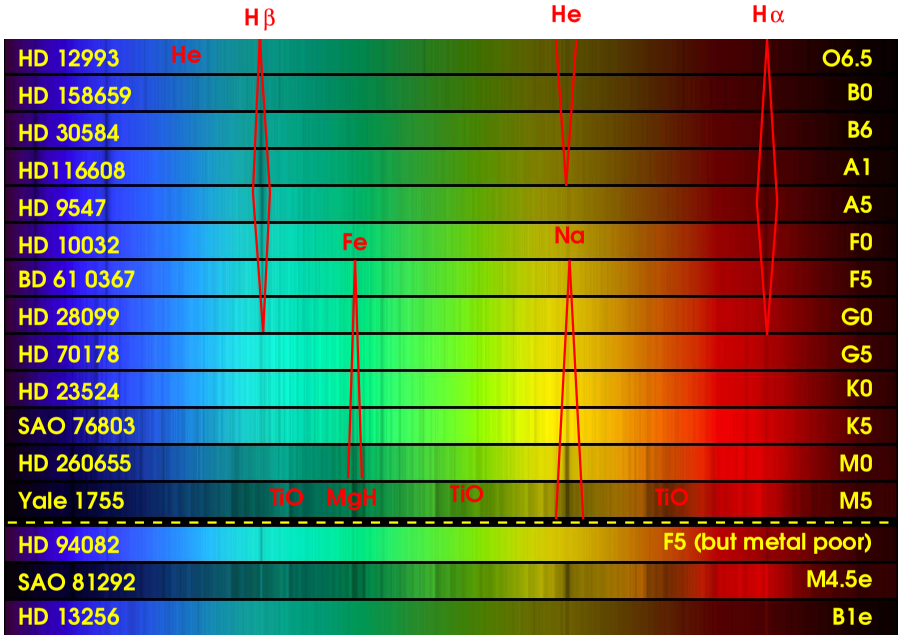

Stars are classified according to the (relative) strengths of their spectral lines.

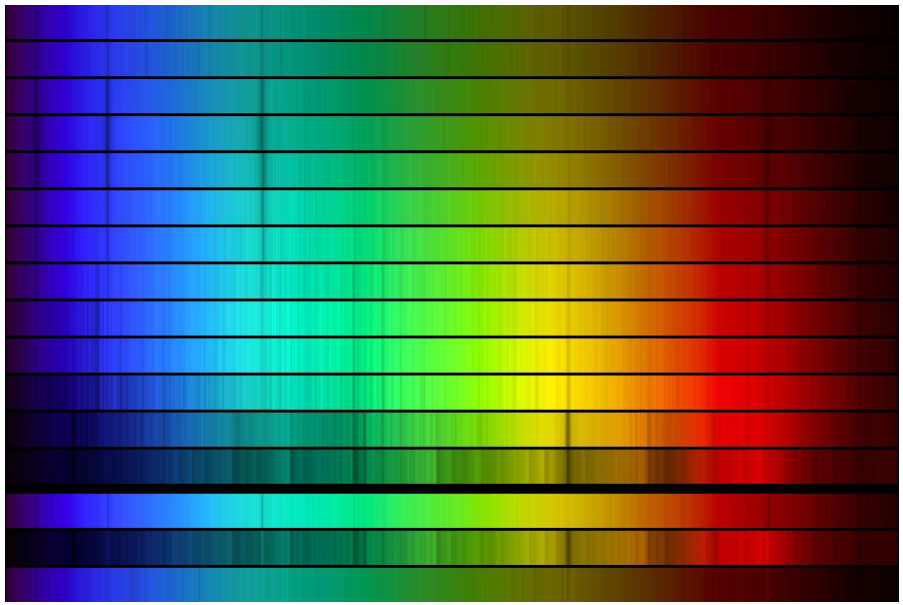

Optical spectra of stars are a Planckian with absorption lines (depending on the temperature of the stars).

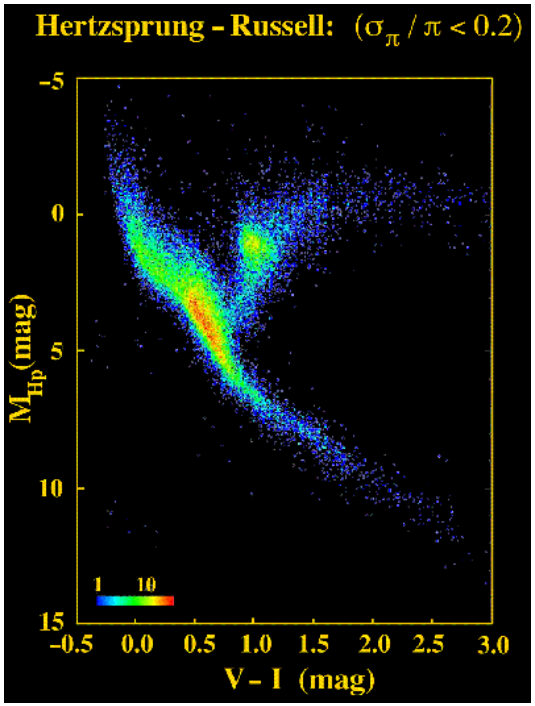

Hertzsprung-Russell diagram of $\sim$ 41500 nearby *HIPPARCOS* stars with parallax error $\sigma(\pi)/\pi < 0.2$

Stellar Structure

Inner structure of stars is described by four differential equations:

Hydrostatic equilibrium: $\frac{\mathrm{d}P}{\mathrm{d}r} = -\frac{GM_r\rho}{r^2}$

Mass conservation: $\frac{\mathrm{d}M_r}{\mathrm{d}r} = 4\pi r^2\rho$

Energy conservation: $\frac{\mathrm{d}L_r}{\mathrm{d}r} = 4\pi r^2\rho\epsilon$

Energy transport:

radiative case:

$$\frac{\mathrm{d}T}{\mathrm{d}r} = \left(-\frac{3}{4ac}\right)\left(\frac{\kappa\rho}{T^3}\right)\left(\frac{L_r}{4\pi r^2}\right)$$

convective case:

$$\frac{\mathrm{d}T}{\mathrm{d}r} \propto \frac{T}{P}\frac{\mathrm{d}P}{\mathrm{d}r}$$

Energy transport by convection when Schwarzschild criterion is met: large radiative gradient (e.g., strong gradient in energy generation), or large κ.

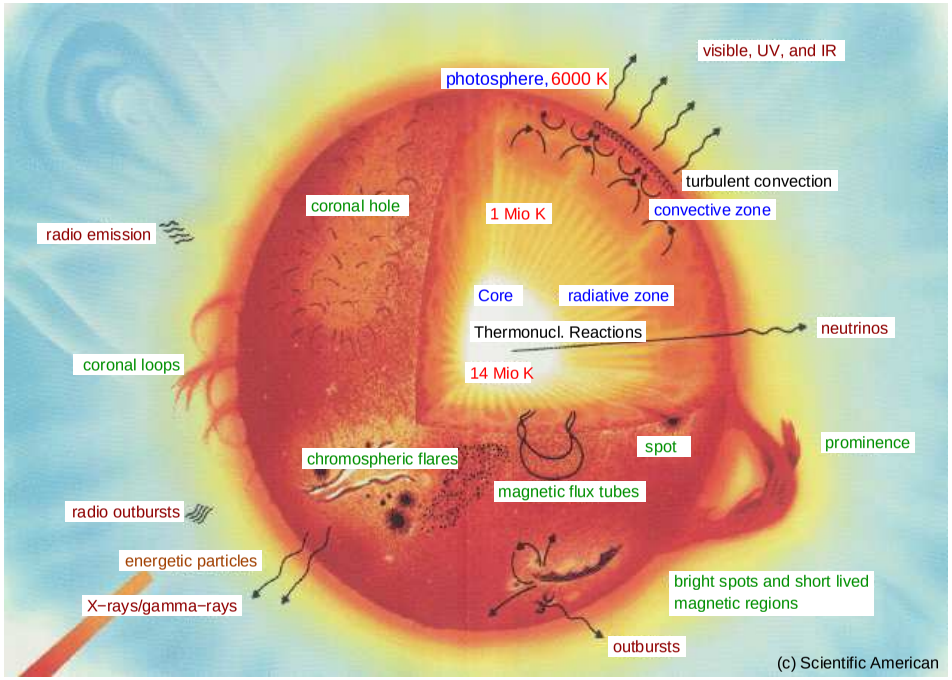

Stellar Structure

Solution of stellar structure equations for main sequence:

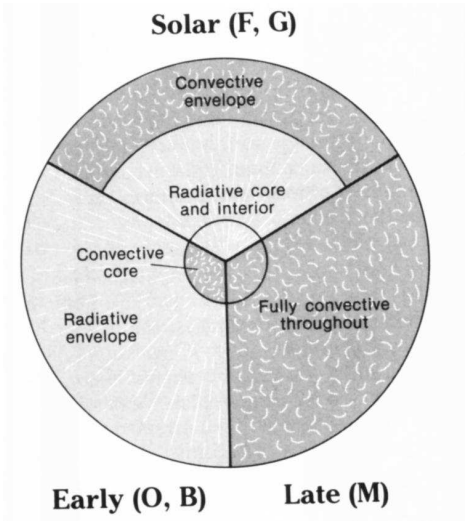

Upper main sequence ($M > 1.5\,M_\odot$):
Core: Temperature very large
$\Longrightarrow$ CNO Cycle $\epsilon \propto T^{15}$
$\Longrightarrow$ convective cores.
Outside of core: radiative equilibrium, no convection.
O- and B-stars: strong stellar winds

Lower main sequence ($M < 1.5\,M_\odot$):
Core: Moderate temperatures
$\Longrightarrow$ pp-cycle ($\epsilon \propto T^6$)
$\Longrightarrow$ cores in radiative equilibrium.
Outer shells: Low temperature
$\Longrightarrow$ large opacity
$\Longrightarrow$ convection

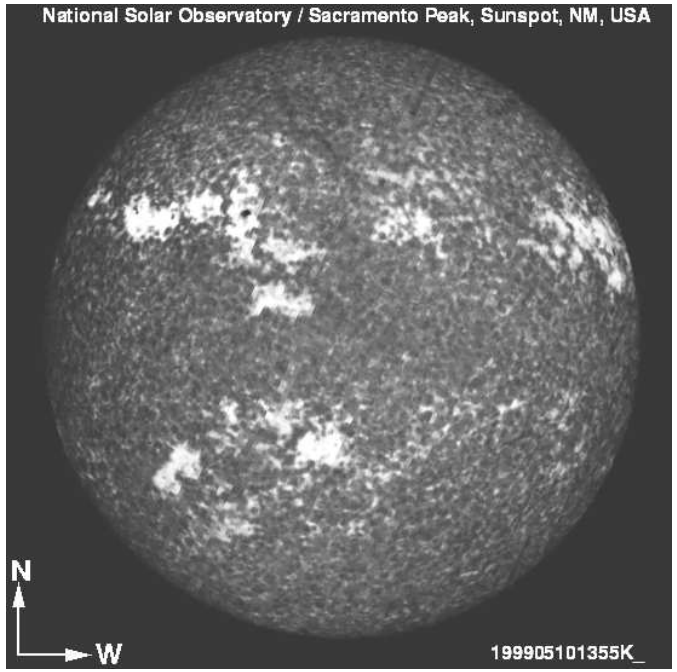

Narrow band ($\Delta\lambda = 1$ Å) spectroheliogram of the Sun in Ca II K line 3933 Å from the National Solar Observatory. Line is formed about 1000 km above photosphere. Bright regions are regions of strong heating, correlated with large magnetic fields.

Sun: 1999 May 10, Optical, Ca K

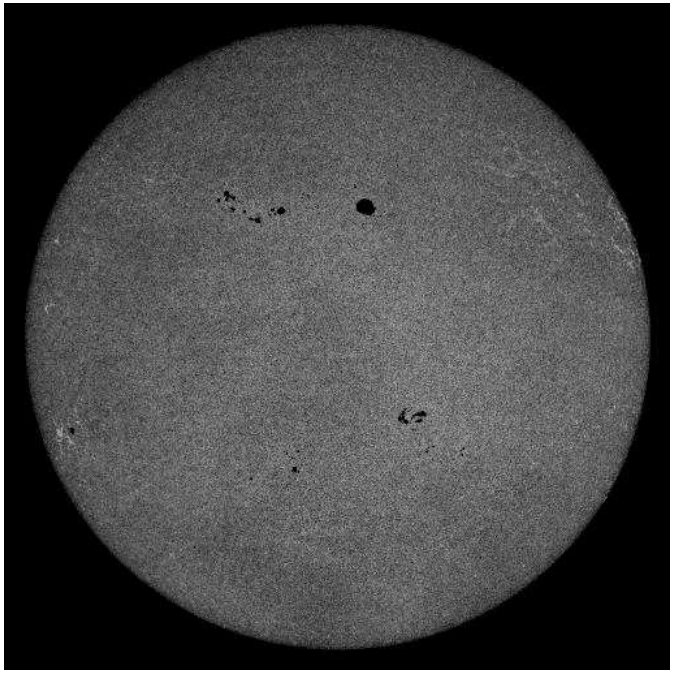

Image of the Sun as a **Doppler tomogram** from the SOHO Michelson Doppler Imager experiment (i.e., image of the Sun in a narrow band optical filter centered on Ni I, 6768 Å); note distribution of sunspots.

Sun: 1999 May 10, Optical, Ca K

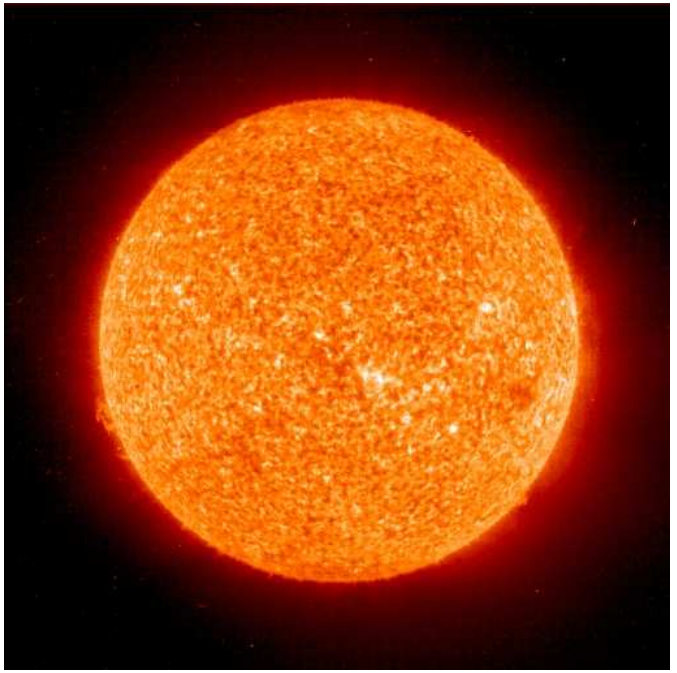

SOHO Extreme Ultraviolet Imaging Telescope (EIT) of the EUV Sun at 304 Å, showing **chromospheric emission** from He II ($T \sim 80000$ K).

Sun: 2008 May 27, EUV

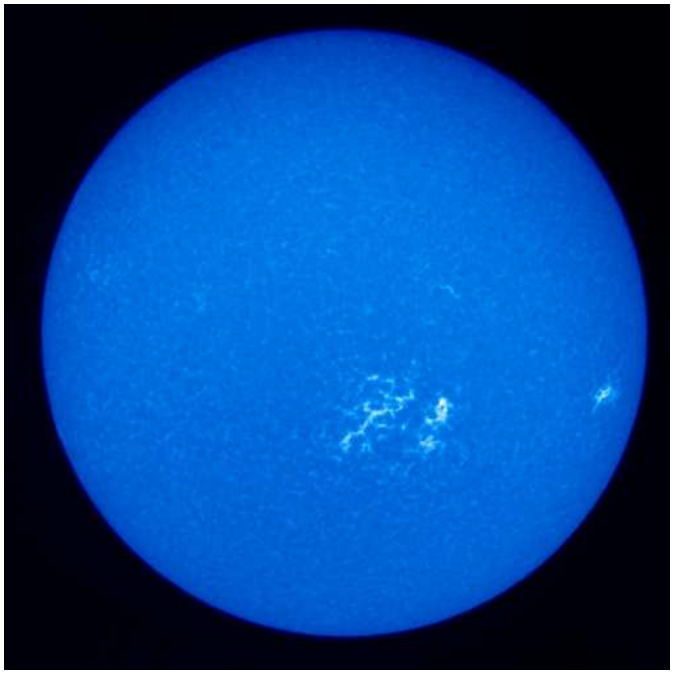

Today the Sun is rather **boring** because we are close to the minimum of the solar activity cycle.

Sun: 2008 May 27, Optical, Ca K [Mauna Loa]

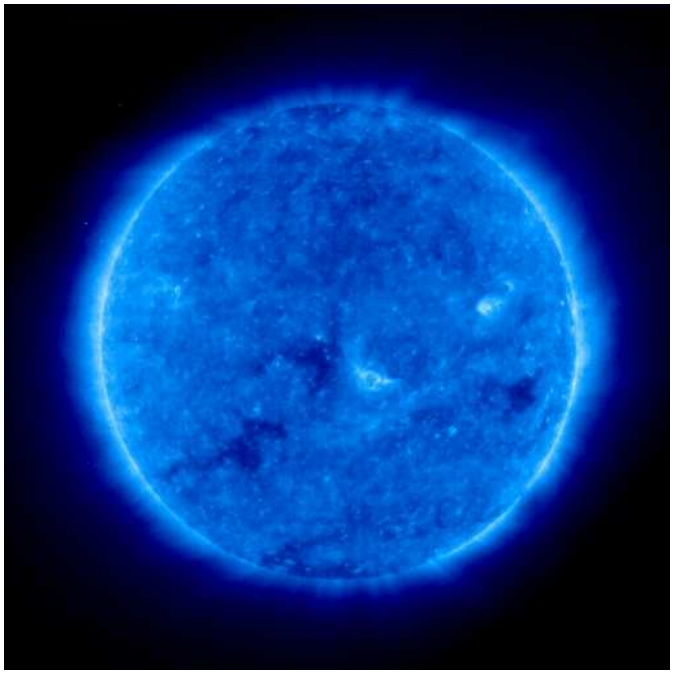

SOHO EIT image of the EUV Sun at 171 Å, showing distribution of emission from highly ionized iron ions (Fe IX/X; $T \sim 10^6$ K) in the **lower corona**.

Sun: 2008 May 27, EUV

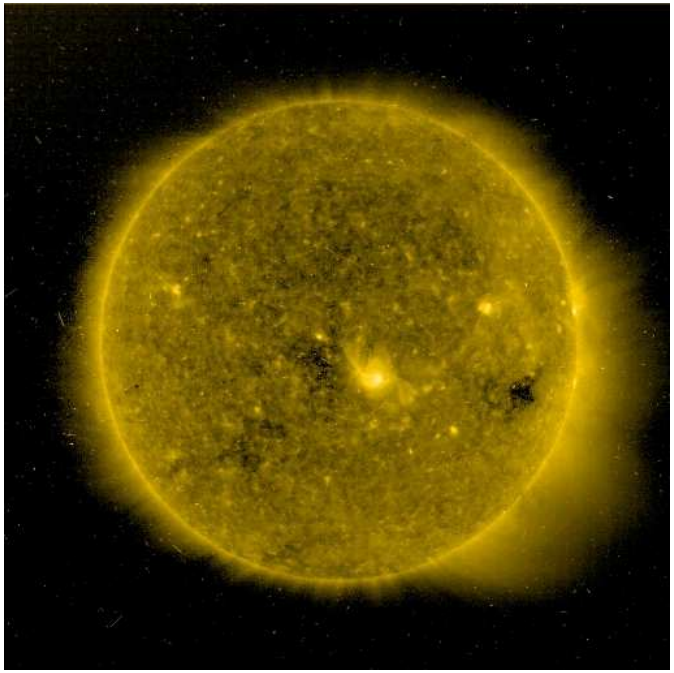

SOHO EIT image of the EUV Sun at 284 Å, showing distribution of emission from Fe XV in the upper corona.

Sun: 2008 May 27, EUV

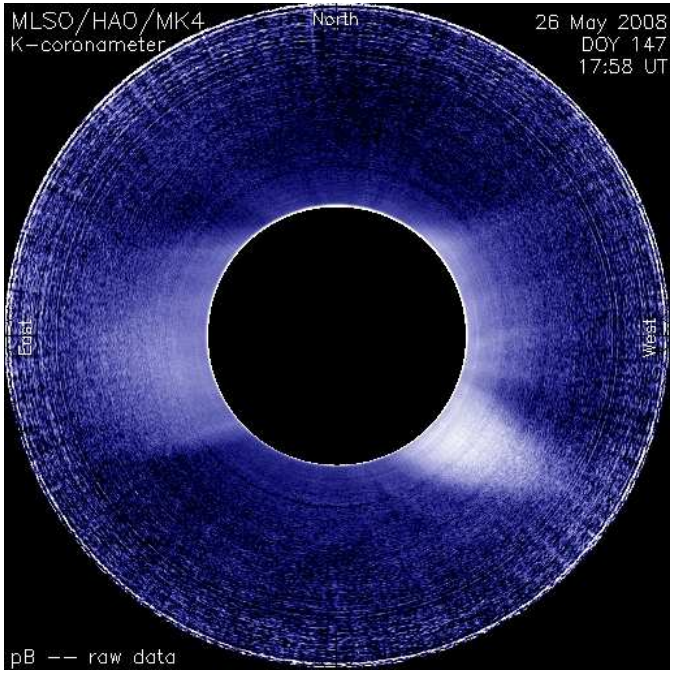

Optical image of the solar corona

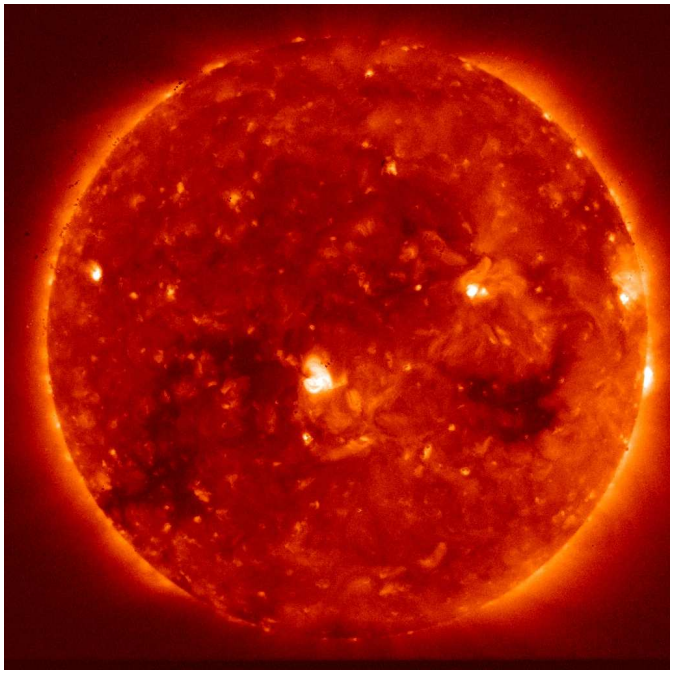

Hinode soft X-ray telescope (SXT) image of the Sun in soft X-rays, showing spatial distribution of the hottest ($T \sim 2 \times 10^6$ K) parts of the outer corona.

5–16

Coronal Spectrum of the Sun

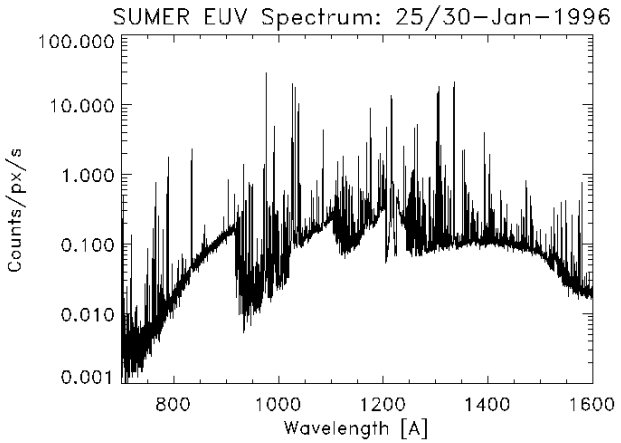

UV spectrum of the solar corona obtained with *SOHO*-SUMER experiment.

$\Longrightarrow$ Optically thin emission line spectrum.

Total X-ray luminosity of the Sun: $L_X \sim 10^{27}\,\mathrm{erg\,s^{-1}}$.

Coronal Plasmas, I

In the coronal model for the ionization equilibrium, the number of ionizations by thermal collisional ionizations is balanced by the number of radiative recombinations (thermal collisional ionization equilibrium; CIE).

$$n_e C_Z(T) n(Z) = n_e \alpha_Z(T) n(Z+1) \tag{5.1}$$

where n: particle number densities.

Therefore

$$\frac{n(Z+1)}{n(Z)} = \frac{C_Z(T)}{\alpha_Z(T)} \tag{5.2}$$

In CIE, the ionization fractions $n(Z+1)/n(Z)$ are a function of temperature only.

Coronal Plasmas, II

Rate coefficients are tabulated in the literature (e.g., Sutherland & Dopita (1993) and references therein), typical forms:

$$C_Z(T) = A_i T^{3/2} \frac{\exp(-I_Z/kT)}{1 + a_i(T/T_Z)}$$

where $T_Z = I_Z/k$, I_Z binding energy, A_i and a_i are fitting coefficients.

For the recombination, radiative recombination and dielectric recombination are important,

$$\alpha_Z(T) = \alpha_{\text{rad}}(T) + \alpha_{\text{diel}}(T)$$

where

$$\alpha_{\text{rad}}(T) = A_{\text{rad}} T^{-\xi_{\text{rad}}} \quad \text{where} \quad \xi_{\text{rad}} \sim 0.6 \ldots 0.9$$

and

$$\alpha_{\text{diel}}(T) = A T^{-3/2} \exp\left(-\frac{T_B}{T}\right)\left[1 + B \exp\left(-\frac{T_i}{T}\right)\right]$$

Coronal Plasmas, III

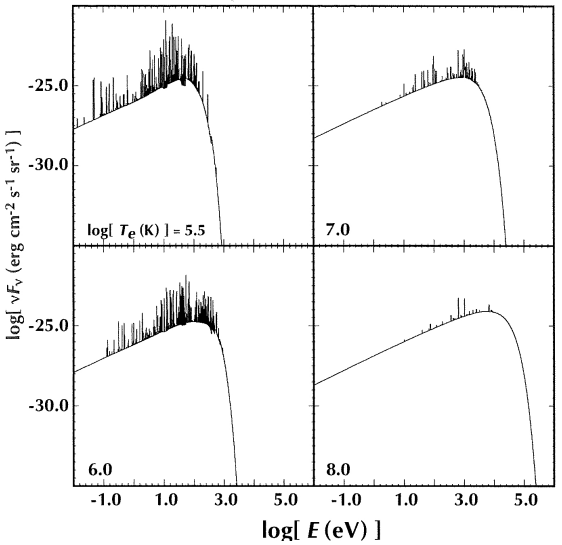

Physics of Corona: Coronal Plasma

(CIE: Coronal Ionization Equilibrium).

Basic assumption: collisional ionization balanced by radiative recombination

Plasma is optically thin

$\Longrightarrow$ Cooling by line emission and thermal bremsstrahlung.

(Dopita & Sutherland, 2003, Fig. 7.2)

Coronal Plasmas, IV

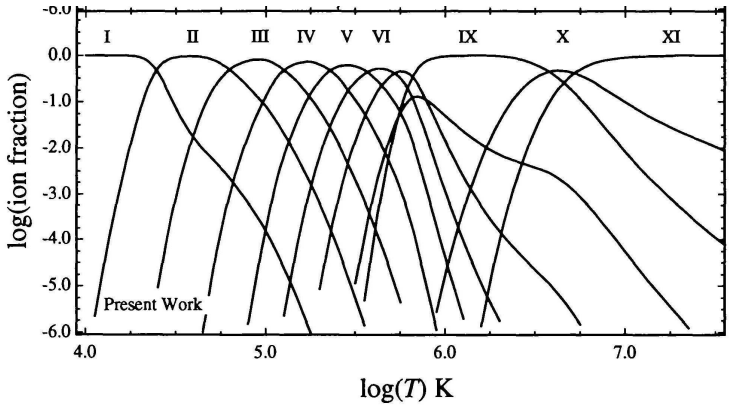

Sutherland & Dopita (1993), Fig. 4

Ionization balance of Neon as a function of temperature in coronal equilibrium.

Only two or three ionization stages are present at each given temperature.

Coronal Plasmas, V

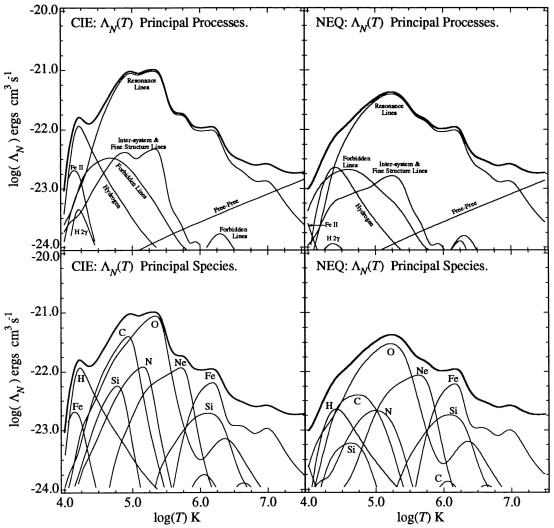

Depending on temperature, different species dominate the cooling

$\Longrightarrow$ Temperature diagnostics.

In addition, using X-ray lines, temperature and density diagnostics become possible (see later, chapter on supernova remnants).

Sutherland & Dopita (1993, Fig. 18)

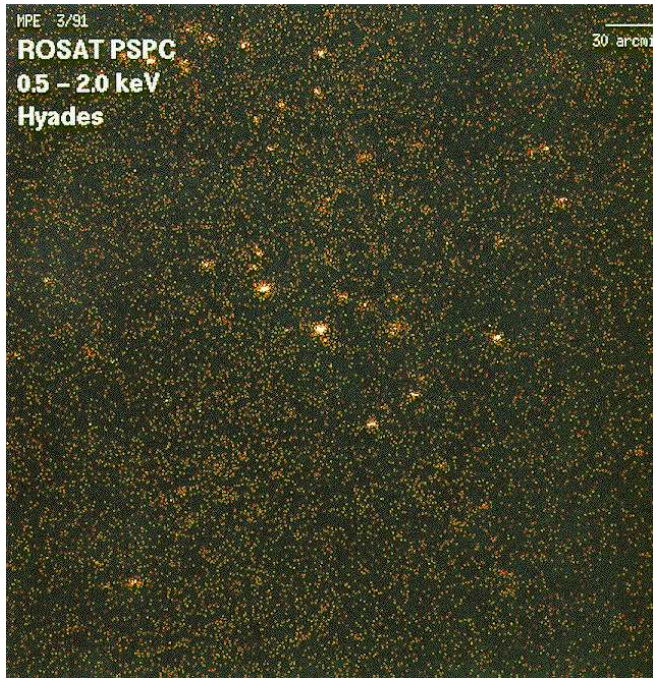

ROSAT image of the Hyades

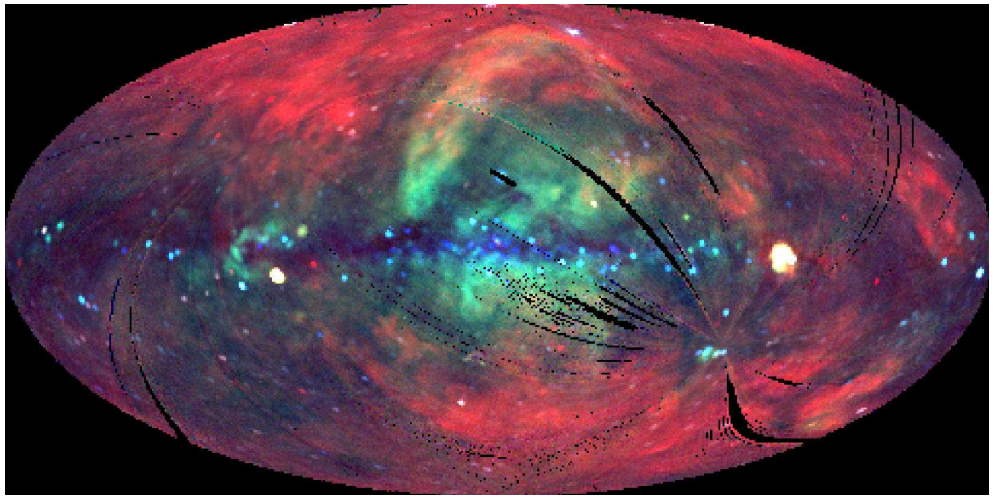

courtesy S. Snowden/HEASARC

ROSAT All Sky Survey contains source concentration towards galactic plane.
Mainly X-ray binaries, but also some stars.

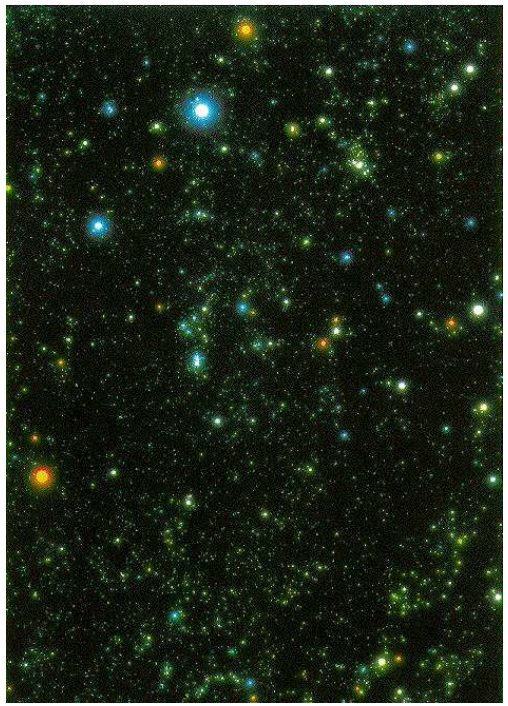

ROSAT image of the Orion region; colors denote the hardness ratio, i.e., the hardness of the X-ray spectrum